MODERN NEUTRON METHODS FOR THE STUDY OF HYDROGEN IN MATERIALS

J. J. Rush and T. J. Udovic

NIST Center for Neutron Research
National Institute of Standards and Technology
100 Bureau Drive, MS 8562, Gaithersburg, MD 20899-8562

Abstract

Neutron scattering and analysis techniques are extremely powerful, often unique, probes for the characterization of the amount, location, bonding states, and dynamics of hydrogen in all classes of materials. Developments over the past decade at the NIST Center for Neutron Research and elsewhere have greatly increased the sensitivity and dynamic range of neutron methods. In this paper, we provide a flavor of the capabilities of modern neutron instrumentation for the study of hydrogen in a number of technologically interesting systems, including metal hydrides, fuel-cell materials, fullerenes, and disordered carbons.

Introduction

The study of hydrogen in materials by neutron scattering and analysis techniques is an important area of materials research. For example, such hydrogen-related studies can facilitate a deeper understanding of the fundamental properties underlying many of today's high-tech materials associated with the field of energy conversion. For the most part, this is due to the novel properties of the neutron and its interactions with matter, especially the different isotopes of hydrogen. The unusually large neutron scattering cross section for hydrogen is routinely exploited by a range of experimental neutron methods in order to probe the amount, location, bonding states, and dynamics of hydrogen in a variety of technologically interesting materials. Developments over the past decade at the NIST Center for Neutron Research (NCNR) and elsewhere around the world have greatly increased the sensitivity and dynamic range of these methods. Figure 1 illustrates the regions of energy-transfer and momentum-transfer space that are currently accessible by NCNR instrumentation. Below, we briefly review these state-of-the-art methods, and provide examples of their recent applications to the study of hydrogen in technology-related materials.
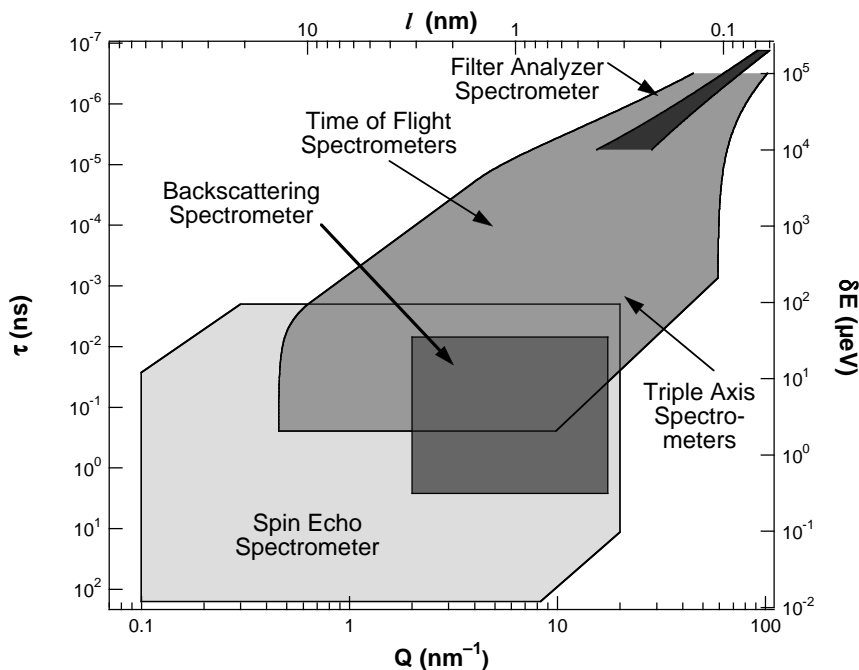

Figure 1: Regions of energy-transfer (δE) [related to the dynamic timescale (τ)] and momentum-transfer (Q) [related to the dynamic lengthscale (l)] space that can be accessed by NCNR inelastic-neutron-scattering instrumentation.

Neutron Methods

Neutron Prompt Gamma Activation Analysis (PGAA)

Neutron Prompt-Gamma Activation Analysis (PGAA) [1] has proved to be useful as a probe of the hydrogen content in materials. The power of this technique as an analytical tool in materials science research has yet to be fully exploited. PGAA is a nondestructive technique for *in situ* quantitative analysis of hydrogen and many other elements based on the measured intensity of element-specific prompt gamma rays emitted upon nuclear capture of a neutron. For the current NCNR instrument, the detection limit of a few μg H permits measurements of dilute concentrations of hydrogen in a large variety of materials.

Neutron Powder Diffraction (NPD)

Neutron powder diffraction (NPD) [2] is invaluable for probing the crystallographic location of hydrogen in materials because of the significant coherent scattering cross section for hydrogen (and deuterium). This is in contrast to x-ray diffraction, which is much less sensitive to the lightest elements. Typically, diffraction patterns are collected from samples containing deuterium instead of hydrogen since the latter possesses a much larger incoherent scattering cross section, resulting in a significant amount of background scattering. The current NCNR high-resolution diffractometer is a versatile instrument with 32 detectors and a choice of two incident Soller collimators as well as three focusing monochromators, Ge(311), Cu(311), and Si(531), depending on the desired resolution, intensity, and range of scattering vector.

Neutron Vibrational Spectroscopy (NVS)

Neutron Vibrational Spectroscopy (NVS) [3] is capable of probing the bonding potentials and sometimes the locations of hydrogen in materials. The recent construction of a next-generation filter-analyzer neutron spectrometer (FANS) at the NCNR with its superior signal/noise ratio is enabling the routine characterization of hydrogen vibrational signatures for much smaller and more hydrogen-dilute samples (*i.e.*, with a detection limit <100 µg H). In a FANS experiment involving hydrogenous materials, incident monochromated neutrons are scattered from the sample, some losing their energy to a hydrogen vibrational excitation, and are counted by a detector bank after passing through a low-energy (≈1 meV) band-pass neutron filter. By varying the incident neutron energy, a vibrational density-of-states spectrum dominated by the hydrogen normal modes is measured. Analysis of the vibrational energy distribution provides insights about hydrogen bonding potentials and interactions. In addition to FANS-type instruments, low-energy (<20 meV) NV spectra are also typically measured using neutron time-of-flight (TOF) instrumentation [4].

Quasielastic Neutron Scattering (QENS)

Besides vibrational studies, the NCNR has also had a longstanding interest in the diffusive and tunneling properties of hydrogen in materials, which can be probed by quasielastic-neutron-scattering (QENS) measurements using triple-axis [5], time-of-flight [4], and backscattering instrumentation [6], which currently cover hydrogen dynamical behavior on timescales ranging from 10^{-8} to 10^{-14} s. QENS [7] simultaneously provides atomic-scale temporal and spatial information on the localized and diffusive motions of hydrogen within a host lattice, and as such, provides valuable insights about the energetics and mechanisms of hydrogen motions in materials. In particular, temperature-dependent and momentum-transfer-dependent quasielastic perturbations in the elastic-scattering peakshape due to hydrogen motions are reflective of the nature and timescale of these motions.

Small Angle Neutron Scattering (SANS)

Small Angle Neutron Scattering (SANS) [8] is a coherent elastic scattering technique useful for the characterization of morphologies of various materials such as porous media, polymers, ceramics, and metals. It can probe inhomogeneities (*i.e.*, local volumes possessing different total scattering lengths) in a material with length scales ranging from atomic (nanometers) to macroscopic (micrometers) dimensions. The very low energies of cold neutrons make them an excellent nondestructive probe capable of penetrating most materials. The difference in sign between hydrogen and deuterium scattering lengths permits the tailoring of the small-angle neutron scattering (*i.e.*, contrast variation) in hydrogenous materials by adjusting the H/D ratio

in the sample or by selective isotopic labelling of portions of a molecule or macromolecule. The NCNR currently has four SANS instruments: an 8-meter and two 30-meter pinhole-collimation instruments that use cold neutrons, and a perfect-crystal diffractometer for ultra-high resolution SANS that uses thermal neutrons. Together, these instruments probe structure in materials over four orders of magnitude ($\approx 1\text{-}10^4$ nm).

Applications

We will now briefly discuss some recent examples of applications of modern neutron methods to the study of hydrogen in a number of materials of current interest.

<u>High-Temperature Protonic Conductors</u>

Perovskite-based high-temperature protonic conductors (HTPC's) have generated increased scientific interest because of their potential use in such areas as solid-oxide fuel-cell technology. In the HTPC's, oxygen vacancies are created either by doping with a lower-valent cation or by non-stoichiometric composition. By steam treatment, the vacancies are filled by the oxygen of the water molecule, and the protons enter the interstitial lattice as OH$^-$ species. The protons in steam-treated samples of strontium cerate (SrCeO$_3$) and strontium zirconate (SrZrO$_3$) aliovalently doped with rare-earth-metal atoms were recently investigated by PGAA, NVS, and QENS. PGAA was used to determine proton concentrations between 0 and 3 mole % in these samples. Figure 2 displays a typical PGAA spectrum for SrZr$_{0.95}$Y$_{0.05}$H$_{0.02}$O$_{2.985}$ indicating the relative sensitivity of the proton-related peak [9].

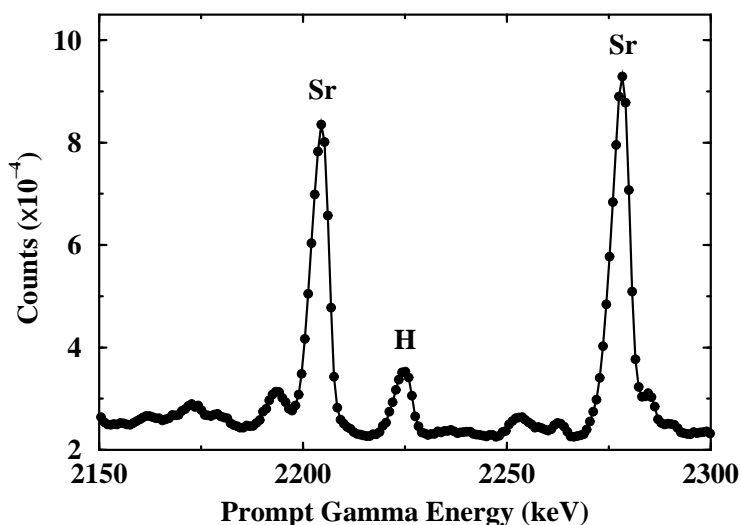Figure 2: PGAA spectrum at 295 K for SrZr$_{0.95}$Y$_{0.05}$H$_{0.02}$O$_{2.985}$ indicating the relative sensitivity of the 2223.23 keV prompt gamma ray emission due to neutron capture by the ^{1}H nucleus (from Ref. [9]).

NVS measurements [10] provided a means of probing the bonding potential experienced by the protons in the lattice. Dopant-related perturbations of the vibrational energies of the OH$^-$ species confirmed the presence of trapping effects by the dopant cations. NV spectra of SrCe$_{0.95}$M$_{0.05}$H$_x$O$_{3\text{-}*}$ (M=Sc, Ho, and Nd) are shown in Fig. 3, where the OH$^-$ bending-mode energy that is associated with trapped protons (located in the region above 80 meV), varied with the type of dopant. The bending-mode energy could be correlated with the size of the dopant cation, generally increasing for smaller cations. Unlike the smaller Sc^{3+} and Ho^{3+} dopant cations, the Nd^{3+} cation is larger than the Ce^{4+} cation. Thus, the only OH$^-$ bending-mode energy
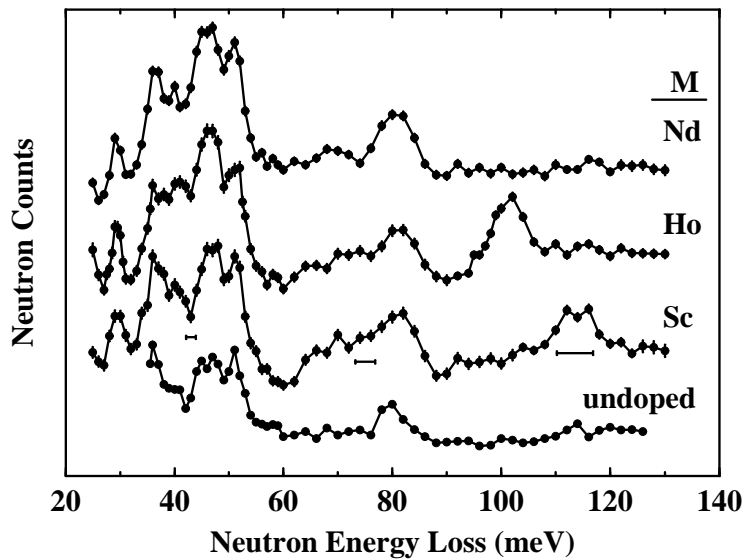
Figure 3: NV spectra at 17 K for $SrCeO_3H_x$ and $SrCe_{0.95}M_{0.05}H_xO_{3-*}$ samples. Hydrogen content $x=0.2$ for the undoped sample, and 1.77, 1.70, and 1.06 for the Sc-, Ho-, and Nd-doped samples, respectively. The instrumental resolution is indicated by the horizontal bars beneath the spectra (adapted from Ref. [10]).

for the Nd-doped sample is near 80 meV, the same as for the undoped sample, suggesting that the OH⁻ species in this case are only associated with Ce^{4+} cations and not near the relatively unfavorable Nd traps. Such differences reflect changes in the lattice potential experienced by the protons due to dopant size, which ultimately affects proton diffusion via the jump rates between potential wells in the lattice.

A QENS study of $SrCe_{0.95}Yb_{0.05}H_{0.02}O_{2.985}$ [11],[12] indicated a two-state model for proton diffusion, with one state representing free diffusion of the protons jumping among lattice oxygens via OH⁻ formations, and the other state representing protons trapped on lower-energy oxygen sites in the vicinity of the Yb^{3+} dopants. In addition to this long-range diffusion, a fast localized reorientation of the free-state OH⁻ ions was observed.

Hydrogen in Buckminsterfullerene

Due to their large spherical shape, buckminsterfullerene (C_{60}) molecules form an fcc lattice, and thus can accommodate a variety of interstitial atomic and molecular species that can greatly influence physical properties. The quantum dynamics of molecular hydrogen (H_2) absorbed by solid C_{60} proved to be particularly intriguing from a fundamental physics viewpoint [13]. The first goal of the $C_{60}(H_2)_x$ study was to locate the interstitial sites for H_2 absorption. This was done by analyzing NPD measurements of D_2 absorbed in C_{60}. Figure 4 illustrates the NPD pattern for $C_{60}(D_2)_x$ at 10 K. Rietveld refinement of the data indicates that the D_2 molecules occupied ≈40% of the octahedral interstices with no occupation of the tetrahedral interstices. The excess scattering from a difference Fourier transform between the Rietveld refinement model of pure C_{60} (without D_2) and the NPD pattern of $C_{60}(D_2)_x$ clearly showed that the D_2 molecules were randomly oriented in the octahedral interstices.

The interstitial D_2 molecules are an almost perfect example of a three-dimensional quantum rotor in a solid with energy levels given by $E_J=BJ(J+1)$, where B is the rotational constant and J is the rotational quantum number. NVS was able to probe the relatively weak interactions of the
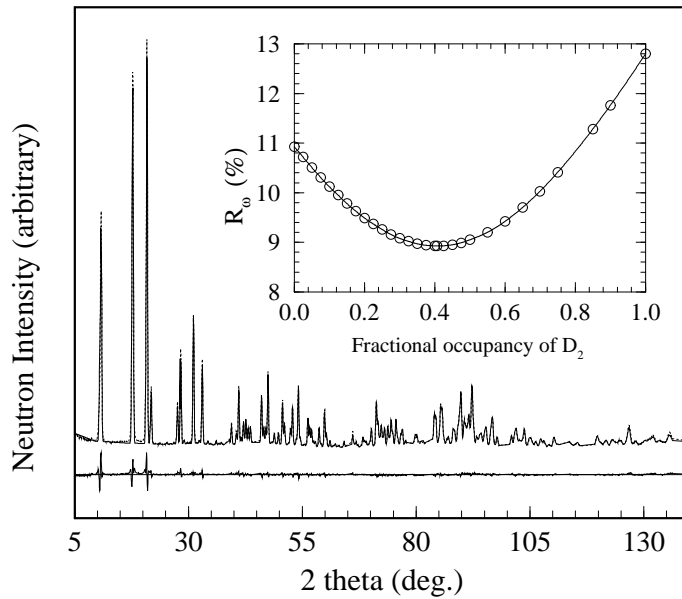
Figure 4: Rietveld refinement and difference plot of the NPD pattern of $C_{60}(D_2)_x$ at 10 K based on a pure C_{60} model with D_2 occupying the octahedral interstices. The inset shows how the goodness of fit (R-factor) changes with the occupancy of octahedral D_2. The best fit is obtained for 40% occupancy (from Ref. [13]).

D_2 rotors with the C_{60} host lattice. Figure 5 shows the TOF neutron-energy-gain spectrum of $C_{60}(D_2)_{0.4}$ at 10 K. The rotational transition is split into two peaks centered at 6.7 and 7.4 meV. Hence, D_2-C_{60} interactions have caused the J=1 rotational level to be split into A (singlet) and E (doubly-degenerate) states. The expected 1:2 ratio of the peak intensities is modified by the thermal population factor at 10 K.
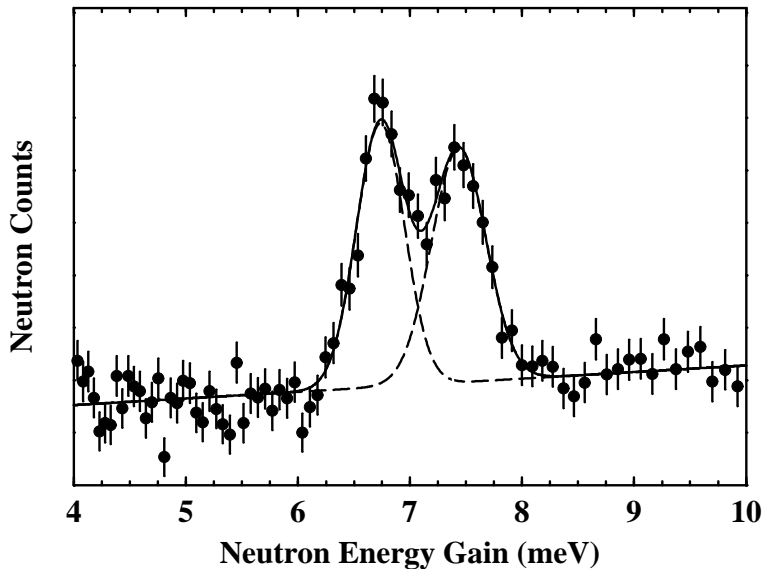

Figure 5: NV spectrum of the J=1→0 rotational transition of D_2 in $C_{60}(D_2)_{0.4}$ at 10 K. The twin peaks at 6.7 and 7.4 meV represent a breaking of the degeneracy into singlet and doublet states due to D_2-C_{60} interactions (from Ref. [13]).

Lithium-ion Battery Anodes

Carbon-based anodes are routinely used in Li-ion batteries. Disordered carbons obtained by pyrolyzing organic solids in an inert gas at T≈973 K exhibit surprisingly large Li-uptake capacities. These materials are composed of graphene fragments, *i.e.*, finite-sized, hexagonal planar sp^2-hybridized carbon networks. However, they also contain a substantial amount of residual hydrogen that presumably terminates the dangling bonds at the edges of the graphene fragments. Understanding the location and bonding states of this hydrogen is crucial since empirical data suggest an upper limit of one excess Li atom per H. The NV spectrum of a disordered carbon sample NT10 (a byproduct of coal tar pitch processing with an H/C atomic ratio of 0.38) was measured [14] to probe the local environments of the residual hydrogen. For comparison, the spectra of coronene $C_{24}H_{12}$, a representative polycyclic aromatic hydrocarbon with a single H atom per edge carbon atom, and polyethylene (-CH2-)$_n$, which provided information on methylene-group modes, were also measured. The three spectra are shown in Fig. 6. The disordered-carbon spectrum is substantially similar to that for coronene, yet quite
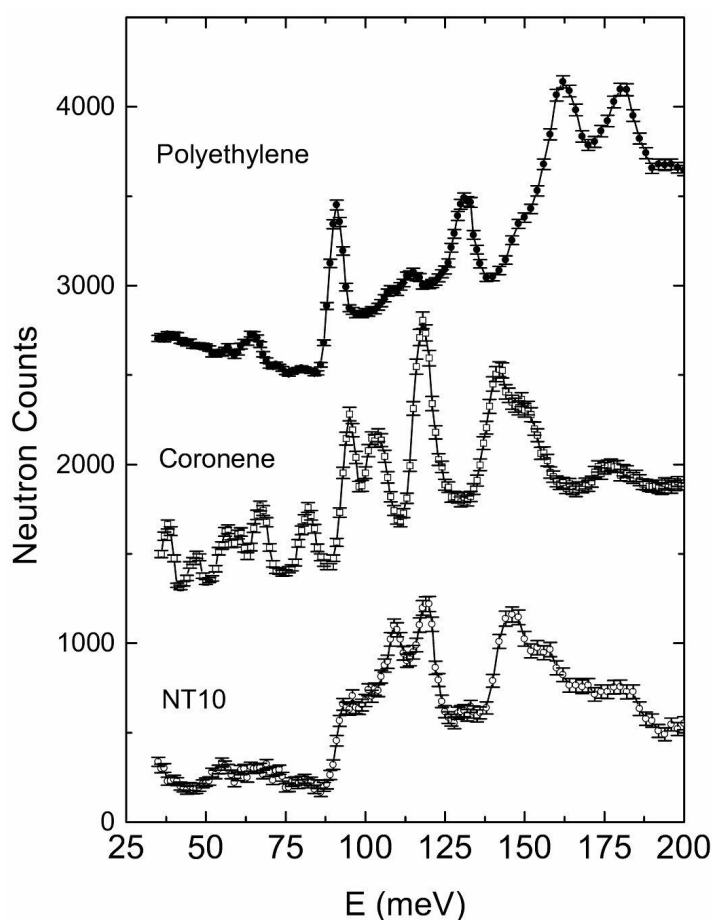

Figure 6: NV spectra of polyethylene, coronene, and the hydrogenous disordered carbon NT10 at 16 K (from Ref. [14]).

dissimilar to that for polyethylene. From this comparison, the intense disordered-carbon peaks between 90 and 125 meV were assigned to aromatic H-atom motions perpendicular to the graphene molecular plane. A broader maximum near 140 meV was assigned to aromatic H-atom in-plane vibrations. These results convincingly demonstrated that the edge C atoms were bonded to a single hydrogen, while the number of CH_2 groups in the disordered carbons was negligible. This was consistent with semiempirical calculations indicating that, in addition to the usual intercalation process where Li is centered over carbon hexagons, Li also may form strongly

polar covalent bonds to H-terminated C atoms at the edges of graphene fragments. This proposed bonding mechanism is possible only if the edge carbons are bonded to a single H atom since two edge H atoms per C atom would result in a chemically inert CH_2 moiety. Thus, NVS measurements along with previous calculations provided a consistent explanation of the large Li uptakes in these materials.

LaNi$_5$-based Metal Hydrides – Batteries and Hydrogen Storage

Hydrogen-metal interactions underlie a variety of critical technological issues such as hydrogen embrittlement, hydrogen storage, nuclear fusion, batteries, heterogeneous catalysis, and future energy production. Materials morphology in the nanoscale regime is one important technological parameter affected by such interactions and can be directly characterized by SANS. For example, using SANS techniques [15], hydrogen distributions and internal strains that accompany hydriding of binary LaNi$_5$ were compared to those in the ternary alloy LaNi$_{4.75}$Sn$_{0.25}$, which is known to have a cycle life superior to that of LaNi$_5$ in electrochemical cells and in hydrogen storage applications. It is known that the unit cell volume of the hydride phase changes more continuously with hydrogen concentration in LaNi$_{4.75}$Sn$_{0.25}$ than in LaNi$_5$, and that the Sn atoms perturb the local chemical potential of the hydrogen atoms. Monte Carlo simulations showed that normal coarsening of hydride zones would be altered, or even arrested, by hydrogen-Sn interactions. SANS difference data for LaNi$_5$D$_x$ and LaNi$_{4.75}$Sn$_{0.25}$D$_x$ for x=2,4 are displayed in a Porod fashion in Fig. 7. The excess SANS intensity shown for partially
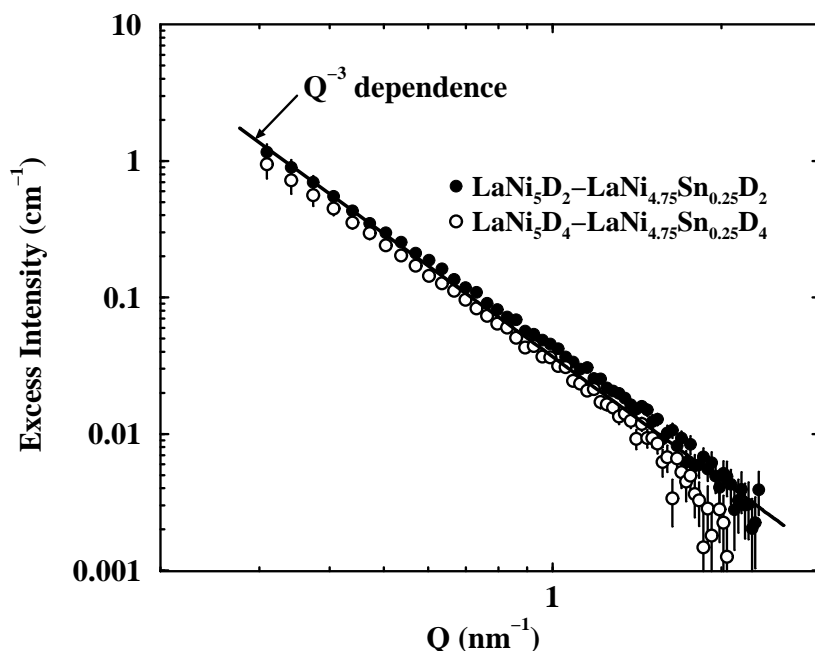

Figure 7: Porod plots of the excess SANS intensity of LaNi$_5$D$_x$ compared to LaNi$_{4.75}$Sn$_{0.25}$D$_x$ for partial (x=2,4) deuterium loadings (adapted from Ref. [15] data).

deuterided LaNi$_5$ is reflective of a less homogeneous distribution of deuterium than in partially-deuterided LaNi$_{4.75}$Sn$_{0.25}$, at least on the spatial scale of 4–15 nm. The nearly Q^{-3} dependence of the excess scattering due to the deuterium-rich regions of LaNi$_5$D$_x$ suggests that these regions have two-dimensional features. The deuterium distribution is found to be the same in fully-deuterided (x=6) LaNi$_5$ and LaNi$_{4.75}$Sn$_{0.25}$, and this distribution matches well the density distribution of the undeuterided samples (i.e., the deuterium distribution is homogeneous). It is

suggested that a more homogeneous deuterium distribution in LaNi$_{4.75}$Sn$_{0.25}$ suppresses the strain gradients that cause decrepitation of the metal hydride.

Perfluorosulfonic-Acid-Ionomer Membranes

Current work at the NCNR on the dynamics of water in perfluorosulfonic-acid ionomers has been prompted by their use as separator membranes in a variety of electrochemical applications such as electrolysis, fuel cells, and batteries. However, the relationship between these polymeric membranes' useful macroscopic properties and their unusual microstructures is still not firmly established. A clear understanding of the protonic conductivity properties of hydrated ionomer membranes requires a detailed physical and chemical understanding of the water-ionomer interaction. Characterization of such a system illustrates the synergism among the different neutron scattering techniques used to probe materials properties. For example, PGAA is used to verify the water content of the hydrated ionomers [16]. Neutron diffraction and SANS are used to characterize the ionomer ordering and micellar-like clustering of water molecules within the ionomer matrix. NVS is used to characterize the hydrogen-bonding interactions of the intercalated water molecules. Finally, QENS is used to characterize the water dynamics. The combined results from these neutron techniques allows for a more thorough understanding of the factors responsible for the favorable protonic conductivity properties associated with these materials. Preliminary QENS spectra [17] for dry (0 H$_2$O/H$^+$) and hydrated (6 H$_2$O/H$^+$) ionomers are shown in Fig. 8. The elastic and quasielastic scattering for
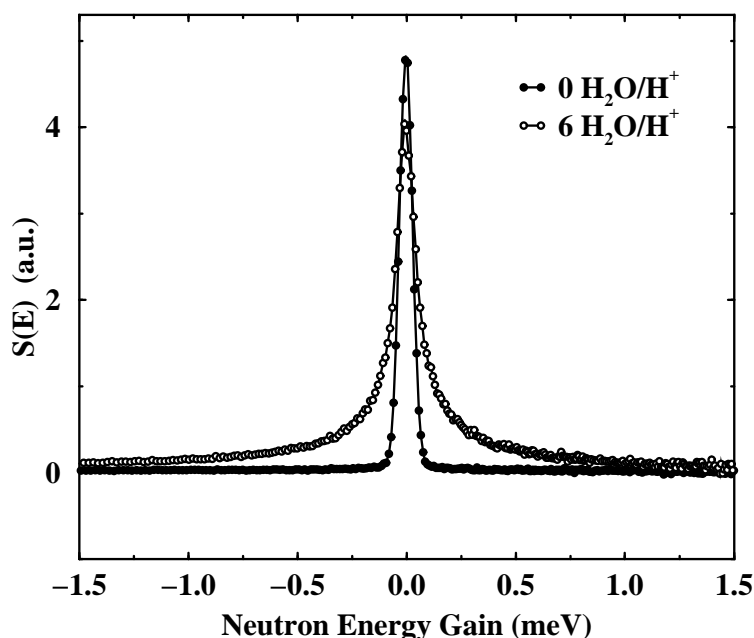

Figure 8: QENS spectra at 300 K and a momentum transfer Q=18.5 nm^{-1} for a perfluorosulfonic-acid-ionomer membrane, dry and after the addition of 6 H$_2$O/H$^+$ (from Ref. [17]).

these ionomers is primarily due to incoherent scattering from hydrogen. The sharp resolution-limited elastic feature for dry ionomer at 300 K represents the bound superacidic protons of the sulfonic acid (-SO$_3$H) sidegroups. Hydration causes a decrease of the elastic feature concomitant with the emergence of a broad quasielastic feature. This indicates that the protons are delocalized by the addition of water molecules to form H$^+$(H$_2$O)$_n$ clusters, a result in agreement with vibrational spectroscopic data. It is clear that the ability of water to abstract the superacidic protons from the sulfonic acid sidegroups is intimately related to the unusual

morphological and favorable conductivity properties associated with this hydrated ionomer. The quasielastic broadening associated with the clusters suggests a dynamical behavior akin to the restricted diffusion of water molecules within a nanosized sphere. This behavior can be correlated with SANS data, which has provided morphological information concerning the size, shape, and spacial arrangement of the clusters [18].

Conclusion

Advances in neutron experimental capabilities have enabled researchers to further their knowledge of hydrogen's role in today's energy-conversion materials. With the development and continual improvement in computing technology, the future focus will be on the more routine integration of *ab initio* computational methods with experimental results in order to gain a more fundamental physical description, from first principles, of technologically important materials properties.

References

1. R. M Lindstrom, "Prompt-Gamma Activation Analysis," J. Res. Natl. Inst. Stand. Technol., 98 (1993) 127-133; R. L. Paul and R. M. Lindstrom, "Determination of Hydrogen in Metals, Semiconductors, and other Materials by Cold Neutron Prompt Gamma-ray Activation Analysis," Mat. Res. Soc. Symp. Proc., 513 (1998), 185-190.

2. J. K. Stalick *et al.*, "Materials Science Applications of the New National Institute of Standards and Technology Powder Diffractometer," Mat. Res. Soc. Symp. Proc., 376 (1995) 101-106.

3. J. R. D. Copley, D. A. Neumann, and W. A. Kamitakahara, "Energy Distributions of Neutrons Scattered from Solid C_{60} by the Beryllium Detector Method," Can. J. Phys., 73 (1995) 763-771.

4. J. R. D. Copley and T. J. Udovic, "Neutron Time-of-Flight Spectroscopy," J. Res. Natl. Inst. Stand. Technol., 98 (1993) 71-87.

5. S. F. Trevino, "The Triple Axis and SPINS Spectrometers," J. Res. Natl. Inst. Stand. Technol., 98 (1993) 59-69.

6. D. A. Neumann and B. Hammouda, "Ultra-High Resolution Inelastic Neutron Scattering," J. Res. Natl. Inst. Stand. Technol., 98 (1993) 89-108.

7. M. Bée, Quasielastic Neutron Scattering—Principles and Applications in Solid State Chemistry, Biology and Materials Science, IOP Publishing Ltd, Bristol (1988).

8. B. Hammouda, S. Krueger, and C. J. Glinka, "Small Angle Neutron Scattering at the National Institute of Standards and Technology," J. Res. Natl. Inst. Stand. Technol., 98 (1993) 31-46.

9. T. J. Udovic *et al.*, "The Applications of Neutron Scattering Methods to the Study of High-Temperature Protonic Conductors," Mat. Res. Soc. Symp. Proc., 548 (1999) 593-598.

10. C. Karmonik *et al.*, "Observation of Dopant Effects on Hydrogen Modes in $SrCe_{0.95}M_{0.05}H_xO_{3-*}$ by Neutron Vibrational Spectroscopy," Solid State Ionics, 109 (1998) 207-211.

11. R. Hempelmann *et al.*, "Quasielastic Neutron Scattering Study of Proton Diffusion in SrCe$_{0.95}$Yb$_{0.05}$H$_{0.02}$O$_{2.985}$," Solid State Ionics, 77 (1995) 152-156.

12. C. Karmonik *et al.*, "Proton Diffusion in Strontium Cerate Ceramics Studied by Quasielastic Neutron Scattering and Impedance Spectroscopy," Z. Naturforschung, 50a (1995) 539-548.

13. S. A. FitzGerald *et al.*, "Quantum Dynamics of Interstitial H$_2$ in Solid C$_{60}$," Phys. Rev. B, 60 (1999) 6439-6451.

14. P. Papanek *et al.*, "Neutron Scattering Studies of Disordered Carbon Anode Materials," J. Physics: Condens. Matter, 13 (2001) 8287-8301.

15. B. Fultz, C. K. Witham, and T. J. Udovic, "Distributions of Hydrogen and Strains in LaNi$_5$ and LaNi$_{4.75}$Sn$_{0.25}$," J. Alloys Compd. (in press).

16. S. K. Young, *et al.*, "Utilization of Prompt Gamma Neutron Activation Analysis in the Evaluation of Various Counterion Nafion Membranes," J. Polym. Sci. Part B: Polym. Phys. (in press).

17. A. M. Pivovar, B. S. Pivovar, T. J. Udovic, and C. M. Brown, private communication with authors, NIST Center for Neutron Research, October 2001.

18. S. K. Young, S. F. Trevino, and N. C. Beck Tan, "Small Angle Neutron Scattering Investigation of Structural Changes in Nafion Membranes Induced by Swelling with Various Solvents," J. Polym. Sci. Part B: Polym. Phys. (in press).